Astron. Astrophys. 348, 737–754 (1999)

ASTRONOMY AND ASTROPHYSICS

Multiple pattern speeds in barred galaxies

I. Two-dimensional models

P. Rautiainen and H. Salo

Department of Physical Sciences, Division of Astronomy, University of Oulu, Oulu, Finland

Received 2 November 1998 / Accepted 21 June 1999

Abstract. We have studied the coexistence of several modes with different pattern speeds in barred galaxies, by a simulation survey exploring a wide range of initial conditions. The high resolution two-dimensional experiments cover the dynamical evolution for about one Hubble time. A remarkable feature of these simulations is that in many cases the spiral structure is clearly visible in the stellar component for several gigayears and weakens so slowly that it can take more than 10 gigayears to become indiscernable even in the direct density plots.

We confirm Sellwood and Sparke's (1988) results that the pattern speed of the spiral arms may differ from that of the bar. However, we find several different variations. There are systems where the bar and the spiral structure are clearly corotating, whereas in others they have different pattern speeds but are probably connected by a non-linear mode coupling as was suggested by Tagger et al. (1987). We have also found models with separate pattern speeds, but without evident mode coupling. Several simultaneous spiral modes can also coexist in the disk, even overlapping in radius. Sometimes the systems have separate inner and outer spirals, the inner corotating with the bar and the outer having a lower pattern speed.

We conclude that similar variation can exist in real galaxies. Some morphological features, like distinct spiral structures with large size differences, can be best explained by separate coexisting patterns. However, there are cases where most of the disk is dominated by one mode. For example, galaxies with well developed outer rings are probably genuine examples of corotating features. It is also possible that in the presence of two or more modes, the appearance of the spiral structure changes considerably in a time scale of about one gigayear while the Hubble type of the galaxy stays the same.

Key words: galaxies: evolution – galaxies: fundamental parameters – galaxies: kinematics and dynamics – galaxies: spiral – galaxies: structure

Send offprint requests to: P. Rautiainen
Correspondence to: pertti.rautiainen@oulu.fi

1. Introduction

The connection between bar and spiral arms has been a subject of debate. In principle, three different scenarios are possible: corotating bar and spiral arms, independent bar and spiral arms possessing different pattern speeds, and also a case where the pattern speeds are different, but the features are still connected by non-linear mode coupling.

There is intuitive evidence for corotating bar and two-armed spiral structures: the spiral arms usually start from the ends of the bar. The intimate bar – spiral connection is also supported by the observations that the fraction of grand design spirals is higher in early type barred galaxies as compared to non-barred ones, and that the size of the two armed spiral in galaxies correlates with the size of the bar (Elmegreen & Elmegreen 1989, 1995). Also the shapes of the outer ring structures fit well with the shapes of periodic orbits near the outer Lindblad resonance (OLR) in barred potentials (Buta & Crocker 1991; Buta 1995). Indeed, in early gas dynamical simulations, where analytical bar potential was used (e.g. Sanders & Huntley 1976), a two armed response to this perturbation, a bar driven spiral, was formed. General gas dynamical simulations can also reproduce outer rings (Schwarz 1981; Combes & Gerin 1985; Byrd et al. 1994). However, these simulations neglect several effects, e.g. self gravitation, so that the assumed bar properties (the pattern speed $\Omega_{\rm b}$, the amplitude $A_{\rm b}$) are not necessarily consistent with the rotation curve.

Usually when individual barred galaxies have been modelled by gas dynamical simulations (with the pattern speed of the bar as an unknown parameter to be deduced), corotation of patterns has been assumed. Although in some cases the spiral response to imposed bar or bar+oval potential, which has been deduced from the observations, has not corresponded with the observations (e.g. Hunter et al. 1988), models which include also the corotating spiral potential have produced an acceptable fit (Lindblad & Kristen 1996; Lindblad et al. 1996; Salo et al. 1999).

On the other hand, if the scheme of bar-driven spiral structure is accepted, it is hard to explain why there are multi-armed barred galaxies, even some where multi-arm structure starts near the ends of the bar. Also flocculent barred galaxies exist (Buta 1995). Sometimes the spiral arms do not start from the ends of the bar but exhibit a clear phase difference. Moreover the ab-

sence of rings in many barred galaxies requires an explanation (Sellwood & Wilkinson 1993).

The second possibility, that bars and spiral arms can be independent features, was demonstrated by the simulations of Sellwood & Sparke (1988, note also that Sellwood 1985 shows a case with different pattern speeds). Their power spectrum of the Fourier $m = 2$ component of the disk surface density shows different patterns speeds for the bar and the spiral arms. They also showed that while the spiral rotates with a lower pattern speed, in most times it still can appear to be connected to the bar.

Although Sellwood and Sparke considered separate pattern speeds being evidence against the dominance of bar-driven spiral structure, an alternative has been suggested: a non-linear mode coupling (Tagger et al. 1987; Sygnet et al. 1988). In this scenario the corotation (CR) of the inner mode (bar) and the inner Lindblad resonance (ILR) of the outer mode (spiral) overlap in radius, which results in a transfer of energy and angular momentum between the modes. Masset & Tagger (1997) presented a simulation that seems to confirm this: clear signs of mode coupling between a bar and a spiral (predicted resonance overlapping, strong beat waves) were present, whereas in a simulation where the bar formation was prevented by a high central mass concentration, also the outer mode more or less disappeared. They propose that mode coupling is a general situation in barred galaxies, a suggestion that we are going to re-examine critically.

Elmegreen et al. (1992a) found that the spiral structure of many galaxies has a prominent $m = 3$ component. Based on their resonance radii determinations, Elmegreen et al. proposed that this $m = 3$ component is a beat mode formed by the normal $m = 2$ component and $m = 1$ component (asymmetry of the two-armed spiral), all having the same pattern speed. They further suggested that this process could produce multi-armed spirals.

In addition to the main bar component, many nuclear bars have been observed (see e.g. Buta & Crocker 1993; Wozniak et al. 1995; Friedli et al. 1996). Friedli & Martinet (1993) showed that at least some of these small scale bars have higher pattern speed than the main bar.

In the current study we have made a large series (about 100 models) of two dimensional N-body simulations, with a wide range of parameters, to address the connection of bar and spiral arms. Our simulations cover the evolution of about one Hubble time. We have used the amplitude spectrum to measure the pattern speeds of the modes and the beat modes, in order to identify possible resonance overlappings. We have also reconstructed the spatial shapes of the individual modes in some of our models, using Fourier decompositions of the surface density from different time steps. Applying this method clearly shows that the modes are either bars/ovals or spirals.

In Sect. 2 we describe the simulation code and summarise the main components of our models. In Sect. 3 we present in detail few models which will highlight the different situations seen in our simulations. We will also shortly present some parameter dependencies we have observed. The discussion and conclusions are presented in the last two sections.

2. Methods

The simulation program uses a two dimensional logarithmic polar grid to calculate the potential. The standard grid geometry has 144 radial and 108 azimuthal cells, whereas some tests were done with both higher and lower resolutions. For comparison we have repeated some simulations with a cartesian potential grid.

The motion of particles is integrated with a time-centered leap frog. The 15 Gyrs simulations are made by using 60 000 time steps. This corresponds to about 150 time steps per rotation period at the distance of one disk scale length while the minimum number of steps per rotation period (very near the center) is about 40. The relative change in total angular momentum during whole simulation is always less than 5×10^{-5} and the total energy is conserved within few percents. Besides stars there is a component of dissipatively colliding test particles, typically 30 000, that we use to model the behaviour of the gas. For more details on the code, see Salo (1991).

Our mass models consist of three main components: self gravitating disk, analytical bulge, and analytical halo. The disk surface density profile follows an exponential law:

$$\Sigma(r) = \Sigma_{\rm c} e^{-r/r_{\rm d}}, \tag{1}$$

where $\Sigma_{\rm c}$ is the central surface density, r the distance from the center and $r_{\rm d}$ the scale length, equal to 3 kpc. We have also made simulations using Toomre disks for comparison and the overall results were essentially similar. The initial extent of the disk is usually 9 scale lengths or 27 kpc, except for some tests with truncation at a smaller distance. Most of the simulations were done with N = 200 000 particles and the most important ones were also ran with 500 000 particles. To further check the effect of the particle number, one mass model was tested by several experiments with N between 32 000 and 1.25 million particles.

Several different values of the initial Toomre's $Q_{\rm T}$- parameter, between 1 and 2, are used, the standard being 1.5. In some models the Toomre parameter was not constant throughout the disk but had a radial dependence:

$$Q(r) = Q_{\rm d} + (Q_{\rm c} - Q_{\rm d})\, e^{-(r/r_{\rm q})^2}, \tag{2}$$

where $Q_{\rm d}$ is the value in the outer disk, $Q_{\rm c}$ the central value and $r_{\rm q}$ defines the radius inside which the transition takes place smoothly. A very similar profile was used by Bertin et al. (1989) in their study of global spiral structures using the modal approach.

The gravitational softening ϵ is usually 375 pc or $1/8$ of the disk scale length. Values $1/16$ and $1/4$ scale length were also used to test the effect of this parameter. In order to suppress possible two-body relaxation effets (see White 1988) we have not used shorter softening lengths, even though this would be tempting when modelling the nuclear region. Another reason is that in two-dimensional simulations the softening parameter

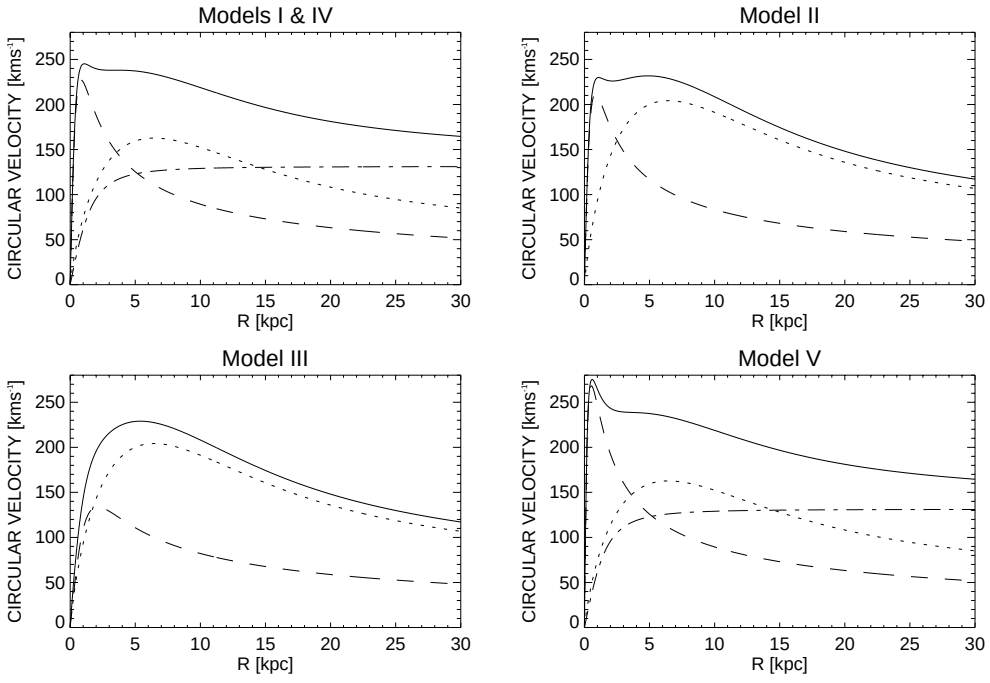

Fig. 1. The initial rotation curves of models I-V, shown by solid curves. Dotted, dashed and dash dotted lines distinguish the contributions from the disk, bulge and halo, respectively.

acts also as a thickness correction (Sellwood 1987) and simulations with very small softening would thus correspond to unrealistically thin disk.

The bulge components are modelled as analytical Plummer spheres, with a circular velocity curve:

$$v_{\rm b}(r) = \sqrt{\frac{GM_{\rm b}r^2}{(r^2+r_{\rm b}^2)^{3/2}}}, \quad (3)$$

where G is the gravitation constant, $M_{\rm b}$ the mass and $r_{\rm b}$ the scale length of the bulge. In few models we used bulges which were composed of two Plummer spheres with different scale lengths.

For the halo, when present, we use an isothermal sphere with a smooth transition to constant core density. This has a rotation curve:

$$v_{\rm h}(r) = v_\infty \sqrt{\frac{r^2}{(r^2+r_{\rm c}^2)}}, \quad (4)$$

where v_∞ is the asymptotic velocity in the infinity and $r_{\rm c}$ the scale of the constant density core. With previously introduced components, we can construct very different models ranging from disk dominated systems to halo dominated ones. The initial rotation curves of the models presented in the next section are shown in Fig. 1. The random velocities of the initial state are created with epicyclic approximation including correction for the asymmetric drift.

We study the morphological evolution from images showing the disk surface density in logarithmic scale. The pattern speed evolution is studied by the amplitude spectra of the Fourier decomposition of the disk surface density in polar coordinates (r,θ):

$$\Sigma(r,\theta) = \Sigma_0(r)\left[1+\sum_{m=1}^{\infty} A_{\rm m}(r)\cos\left(m(\theta-\theta_{\rm m}(r))\right)\right], \quad (5)$$

where $A_{\rm m}(r)$ and $\theta_{\rm m}(r)$ are the Fourier amplitude and phase angle, respectively. The amplitude spectra (see e.g. Sellwood & Athanassoula 1986; Masset & Tagger 1997) are formed using data from 2.5 gigayear intervals. These intervals are long enough to give a good resolution (about $1.26{\rm kms}^{-1}{\rm kpc}^{-1}$ for $m=2$ modes) of pattern speeds and short enough to show the evolution of individual modes. In these simulations, the $m=2$ modes are the strongest ones, but we have also paid attention to evolution of other modes. We estimated the noise level of the amplitude spectra by making a simulation with 200 000 massless particles moving in the halo potential. The highest $m=2$ peak was about 0.03 (0.02 for $m=4$), whereas more typical values were around 0.01. We have adopted 0.03 as a lowest contour level in the $m=2$ amplitude spectra we show here. However, when tabulating the pattern speeds of different modes, we counted features even below this level, because some of them are evidently real (they are present in several time intervals).

To identify the possible resonances related to modes, we have calculated the circular frequency Ω and the epicyclic frequency κ from an axisymmetrized rotation curve and overplotted curves showing Ω, $\Omega \pm \kappa/m$. In the case of $m=2$ modes, we have also plotted the $\Omega-\kappa/4$-curve to determine the radius of inner 4/1-resonance. The axisymmetrized rotation curve is calculated from the radial forces in the middle of the time interval. We have also used the Fourier components in making animations of the density distribution. This is far more economical than saving either the particle positions or surface densities for several hundred time steps. We have found these animations very useful because the individual snapshots of density distribution can sometimes be misleading.

We have predicted the wave frequencies $\omega_{\rm beat}$ and the azimuthal wave numbers $m_{\rm beat}$ of the beat modes from the corresponding term of the parent modes using the following selection rules (Tagger et al. 1987; Masset & Tagger 1997):

$$\begin{cases} \omega_{\rm beat} = \omega_{\rm parent1} \pm \omega_{\rm parent2} \\ m_{\rm beat} = m_{\rm parent1} \pm m_{\rm parent2}, \end{cases} \quad (6)$$

where the pattern speed $\Omega_{\rm beat} = \omega_{\rm beat}/m_{\rm beat}$. In this study we usually display pattern speed instead of wave frequency, except in the case of $m = 0$ modes.

Sellwood & Athanassoula (1986) studied the shape of the modes in their simulations by using spatial and temporal Fourier analysis of the disk surface density distribution in terms of logarithmic spiral decomposition. We do the same but construct the actual shapes of the modes in a bit more straightforward way. First we determine the pattern speed of each mode by using the amplitude spectrum. Then we use this pattern speed to rotate the Fourier phase angles in different time steps so that the orientation of the mode should be the same. Then we calculate the perturbed density ($m = 2$ and $m = 4$ components) at each time step in a polar grid having 30 radial and 100 azimuthal cells. The final mode shape is acquired by summing the perturbed density tables and dividing the resulting table by the number of used time steps. This procedure gives the shape of the mode if the number of used data sets is high enough and the time interval is so long that the amplitude of ghost images produced by other modes are suppressed. To meet these conditions we took data from 101 time steps in a 2.5 gigayear interval. Naturally, the pattern speed of the mode must be practically constant during this interval.

There are three evident shortcomings in the present simulations. First, the three dimensional evolution, especially the possible formation of a boxy bulge (Combes & Sanders 1981; Raha et al. 1991) is neglected. The additional slow-down process of the bar rotation due to the interaction with halo particles (Little & Carlberg 1991; Debattista & Sellwood 1997) is also out of scope of present experiments. The third missing process is the formation of massive central concentration as a result of gas flow to the center (Friedli & Benz 1995; Norman et al. 1996), which can lead to a destruction of the bar.

3. Results

We have searched through a large parameter space and have chosen five models to characterize different evolutionary trends we have observed. The fundamental parameters of the presented models are listed in Table 1. We will first concentrate on the evolution of these models and analyse the dynamics behind that. Then we will make remarks on various parameter dependencies we found when making the survey. Finally we will construct the shapes of individual modes in two of the simulations and also briefly study the evolution of the gas component in our models.

Table 1. Fundamental model parameters. Masses are in units of $10^{10}{\rm M}_\odot$, and radii in kiloparsecs. Halo masses are for inside 5 disk scale lengths, 15 kpc, and $r_{\rm c} \approx 1.9$ kpc. The last column shows the radial force due to disk divided by the total radial force at the distance of two disk scale lengths.

Model	$M_{\rm d}$	$M_{\rm b}$	$R_{\rm b}$	$M_{\rm h}$	$\frac{F_{\rm rdisk}}{F_{rtot}}$
I & IV	4.8	1.9	0.6	6.0	0.46
II	7.5	1.6	0.6	0.0	0.77
III	7.5	1.6	3.0	0.0	0.78
V	4.8	1.9	0.3, 0.6	6.0	0.46

3.1. Pattern speed multiplicities

We have identified three basic types of pattern speed multiplicities in our simulations: 1) bar and spiral arms with different pattern speeds, 2) corotating bar and spiral arms and 3) a nuclear bar rotating faster than the main bar. The type 1) has two variants: systems where the modes are coupled and systems where they seem to be independent. The type 3) is usually associated with either type 1) or type 2) structure, but not vice versa; nuclear bars are not present in all models. In the next subsections we present few examples showing these phenomena.

3.1.1. Model I

Model I consists of a Plummer bulge, an exponential disk and a halo. The contribution of the bulge and the halo to the rotation curve is about the same as that of the disk in the distance of about 8 kpc (see Fig. 1), otherwise it is higher.

Fig. 2 shows the morphological evolution of this model. In the beginning of the simulation there is a transient multiarmed spiral in the outer disk while the bar is forming in the inner parts. At about the same time as the bar reaches its maximum strength ($T \approx 5$ Gyrs), a two armed spiral component is seen. During the further evolution of the system, the bar grows until it stabilizes and the spiral structure weakens so that it cannot anymore be seen in direct density plots.

The pattern speeds and amplitudes of various features can be seen in the amplitude spectra of Fig. 3. The evolution after the bar formation (at $T \approx 4.0$ Gyrs) can be divided to different stages. In the first stage (5.0–7.5 Gyrs) the pattern speed of the bar is decreasing and the evolution of the system is fast. In the second stage (7.5–10.0 Gyrs) the pattern speed of the bar has become almost constant and there are several spiral modes with lower pattern speed than that of the bar. In the last stage, towards the end of the simulation, the spiral modes, except one, become very weak (and in still longer simulations even this mode disappears).

We try to recognize the possible mode couplings using the circular and epicycle frequencies determined by the linear approximation. One of the spiral modes (S3 in the figure), with pattern speed 9.9 kms^{-1}kpc^{-1}, has its ILR relatively close to the corotation of the bar and so is an example of a mode that might be coupled with the bar via the mechanism suggested by Tagger et al. (1987). Later, this mode becomes stronger and the

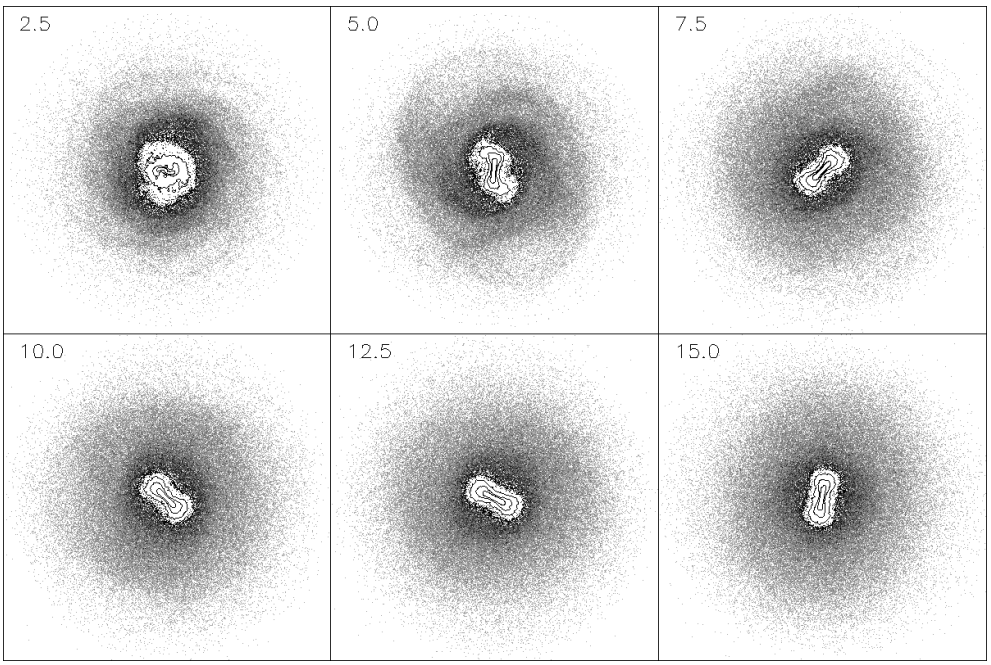

Fig. 2. The evolution of Model I. The disk surface density is shown in logarithmic scale. The innermost areas are presented as contours and the outer disk as shades of grey. Time in gigayears is shown in upper left corner of each frame. The width of the frames is 54 kpc $= 18$ disk scale lengths. Rotation of the disk is counter clock-wise.

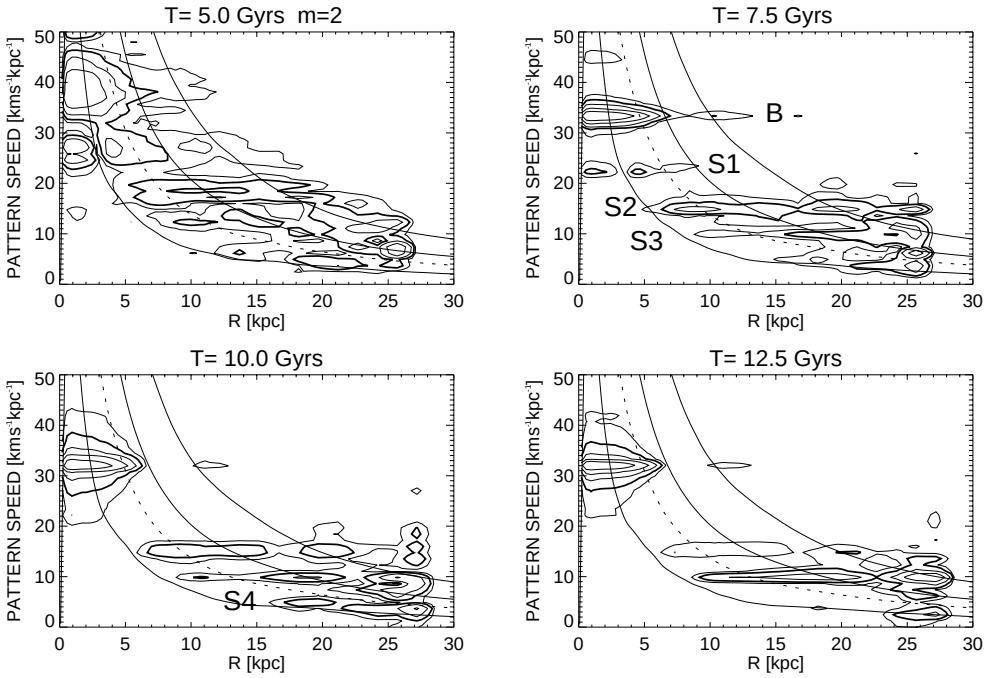

Fig. 3. The amplitude spectra of m=2 Fourier component of Model I in 2.5 gigayear time intervals centered on times T = 5.0, 7.5, 10.0 and 12.5 gigayears. The bar and the different spiral modes are indicated in T = 7.5 Gyrs frame by B and S1 - S4, as in the text. The contour levels are 0.03, 0.06 (drawn with thicker line), 0.12, 0.24 and 0.48. The full lines show the Ω and $\Omega \pm \kappa/2$ curves and the dashed line the $\Omega - \kappa/4$ curve, calculated from the radial forces at the middle of the indicated time interval.

situation indeed resembles the non-linearly coupled system of Masset & Tagger (1997).

The ILR – CR mode coupling looks at first very appealing although it does not explain the intermediate modes, one of which (S2) is initially even stronger than the suspected coupled mode. The complexity of the situation becomes more evident when comparing in more detail the resonance radii ot the modes, shown in Table 2. The ILR (more exactly the outer ILR) of the boosted mode at T = 7.5 gigayears is almost 20% outside the CR of the bar. However, due to the strength of the bar, the epicycle approximation is not very precise and so the overlapping may actually be closer.

A very interesting phenomenon is seen when comparing the inner 4/1 and corotation resonance radii of different modes, namely the $r_{4/1}$ of a slower mode seems to be very close to $r_{\rm CR}$ of a faster mode (B – S1, S1 – S2 and S2 – S3). At T=12.5 gigayears the fastest of the intermediate modes (S1) falls below the lowest contour level of Fig. 3, but it can still be found if a lower cut-off level is used. An alternative to the CR – 4/1 coupling is that the bar feeds two spiral modes (S2, S3) through CR – ILR coupling, one having ILR inside the corotation and the other outside it. In addition to previously discussed modes, by $T = 10$ Gyrs there is also a mode, S4, with pattern speed of

Table 2. The $m = 2$ modes, their resonance radii and maximum amplitudes in Model I for different time intervals. The pattern speeds Ω_p are in kms^{-1}kpc^{-1} and radii in kiloparsecs. The modes are identified as B (bar) and S (spiral).

T	Mode	Ω_p	$r_{\rm ILR}$	$r_{4/1}$	$r_{\rm CR}$	$r_{\rm OLR}$	$A_{\rm max}$
7.5	B	33.2	2.3	4.7	6.6	10.0	1.00
	S1	22.4	3.4	6.6	9.2	14.4	0.08
	S2	14.8	5.5	9.3	13.5	20.0	0.26
	S3	10.0	7.8	13.2	18.8	27.5	0.19
10.0	B	32.0	2.4	4.8	6.8	10.3	0.85
	S1	22.3	3.4	6.7	9.2	14.7	0.06
	S2	14.9	5.4	9.5	13.2	19.9	0.11
	S3	10.0	7.4	13.1	18.8	27.3	0.26
	S4	4.9	12.9	24.5	33.0	51.1	0.10
12.5	B	32.0	2.4	4.8	6.8	10.4	0.93
	S1	22.3	3.4	6.6	9.4	14.6	0.014
	S2	15.3	5.4	9.2	12.8	19.6	0.07
	S3	9.9	7.9	13.0	19.0	27.8	0.41

about 5 kms^{-1}kpc^{-1}, which has a CR – ILR overlapping with S2. This mode disappears later.

3.1.2. Models II and III

Model II does not have a halo and to keep its inner rotation curve closely similar to that of Model I, the disk mass is higher. The importance of the disk/halo mass ratio is demonstrated by Fig. 4 that shows the time evolution of the density distribution and Fig. 5 that shows the amplitude spectra. Although the rotation curves and hence the circular and the epicycle frequency curves are quite similar to Model I, the pattern speed of the bar is dramatically lower. Another difference is that the slower modes, which are present outside the OLR of the bar, are very weak and even the strongest one weakens below the lowest contour value of Fig. 5 by 10 Gyrs. Therefore, one mode dominates this system and reaches even beyond its OLR. Inside the corotation resonance it has a bar shape and further out the Fourier phase angles turn so that it forms a spiral. As can be seen from Table 3, there are fewer resonance overlappings than in Model I and most of them are probably coincidental. The closest of these overlappings is the OLR – ILR overlapping between the bar and the mode S2 by $T = 5$ Gyrs.

Model III resembles Model II so that it has no halo and the total mass of the disk is larger than in Model I. The scale length of the bulge is now larger and so the inner rotation curve is shallower than in previous models. The evolution of this model is very similar to Model II and is not shown here. As in the previous cases, the bar pattern speed is not the only one present but there are slower modes in the outer disk. In this case, only one of them is above the lowest contour level of the amplitude spectrum, shown in Fig. 6. The resonance radii, calculated from the epicycle approximation, do not support mode coupling, at least not in the form favoured by Masset & Tagger (1997): as can be seen from Fig. 6, the inner Lindblad resonance of the outer mode is outside the outer Lindblad resonance of the bar.

Table 3. The $m = 2$ modes, their resonance radii and maximum amplitudes in Model II for different time intervals.

T	Mode	Ω_p	$r_{\rm ILR}$	$r_{4/1}$	$r_{\rm CR}$	$r_{\rm OLR}$	$A_{\rm max}$
5.0	B	16.0	5.5	8.6	10.5	14.2	0.71
	S1	7.4	10.6	14.3	18.2	26.0	0.059
	S2	4.9	14.2	19.0	24.9	34.0	0.079
	S3	3.8	16.7	23.2	30.7	40.2	0.051
7.5	B	13.6	6.6	9.6	11.8	16.1	0.67
	S1	7.4	10.9	14.5	18.2	25.7	0.024
	S2	4.9	14.3	19.3	24.4	33.8	0.042
10.0	B	12.3	7.2	10.3	12.7	17.2	0.66
	S1	7.4	11.0	14.4	17.9	25.2	0.022
	S2	4.9	14.2	18.9	24.1	33.9	0.040
	S3	3.8	16.7	23.6	30.1	41.1	0.028
12.5	B	11.7	7.6	10.7	13.1	17.6	0.48
	S4	6.2	12.2	16.3	20.4	28.8	0.027
	S3	3.7	17.1	23.3	29.8	40.7	0.028

Table 4. The $m = 2$ modes, their resonance radii and maximum amplitudes in Model III for different time intervals.

T	Mode	Ω_p	$r_{\rm ILR}$	$r_{4/1}$	$r_{\rm CR}$	$r_{\rm OLR}$	$A_{\rm max}$
5.0	B	16.2	3.9	8.8	10.5	13.9	0.93
	S1	12.4	8.0	10.5	12.6	17.0	0.023
	S2	4.4	15.4	20.6	26.5	35.9	0.12
7.5	B	14.7	6.5	9.3	11.2	14.8	0.77
	S3	8.6	10.3	13.2	16.2	21.9	0.015
	S2	4.5	14.5	20.7	25.9	35.6	0.096
10.0	B	14.8	6.9	9.3	11.3	14.9	1.0
	S4	3.8	17.1	22.9	28.8	39.9	0.067
12.5	B	14.1	7.3	9.6	11.5	15.3	0.67
	S3	8.7	10.1	13.2	16.1	21.7	0.022
	S4	3.8	16.8	22.9	29.1	39.5	0.034

The spiral structure is clearly formed from two parts (see the $\Omega_{\rm B}$ contours in Fig. 6): the inner pattern corotating with the bar dominates even beyond its OLR, while the slower one appears only in the outermost disk.

The differences between Model I and models II and III can be partly explained by the difference of $Q_{\rm T}$ -parameter in the domain of the spiral structure. By $T = 10$ Gyrs $Q_{\rm T}$ is around 3 in Model I whereas in models II and III the outer disk is so heated that $Q_{\rm T} \geq 5$. This will efficiently suppress the outer modes. The other reason is that because the pattern speed of the bar is lower, the domain of the bar mode becomes so large that there is simply less space available for the slower modes.

3.1.3. Models IV and V

Many of our simulations have nuclear bars in their early evolution. Often these features disappear when the main bar forms: the nuclear bar becomes aligned with the main bar and rapidly loses its identity. In cases where the nuclear bar survives the formation of the main bar, two different scenarios are seen. In

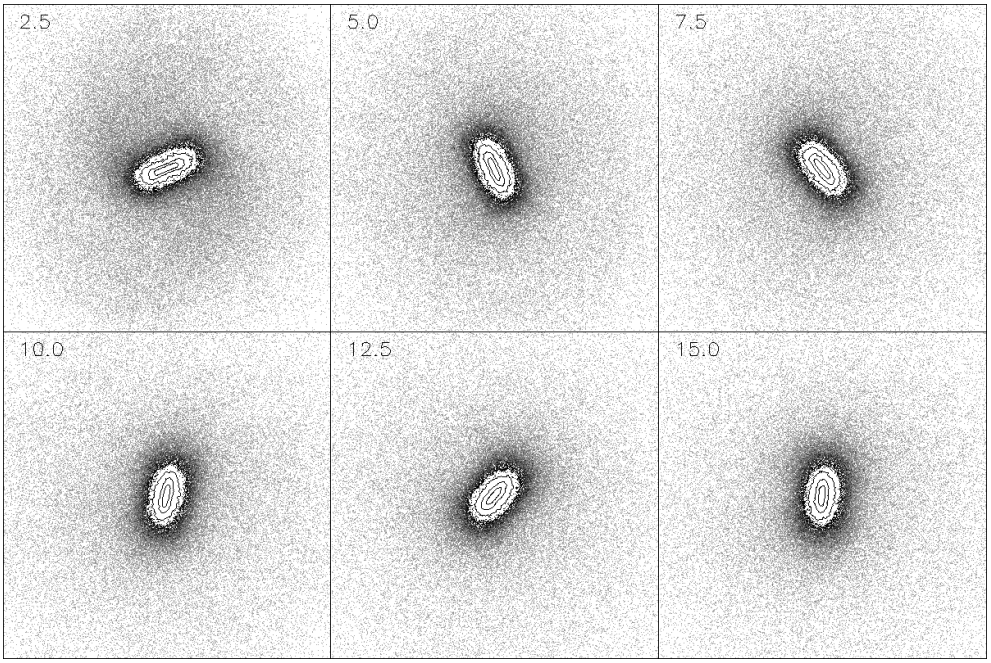

Fig. 4. The evolution of Model II.

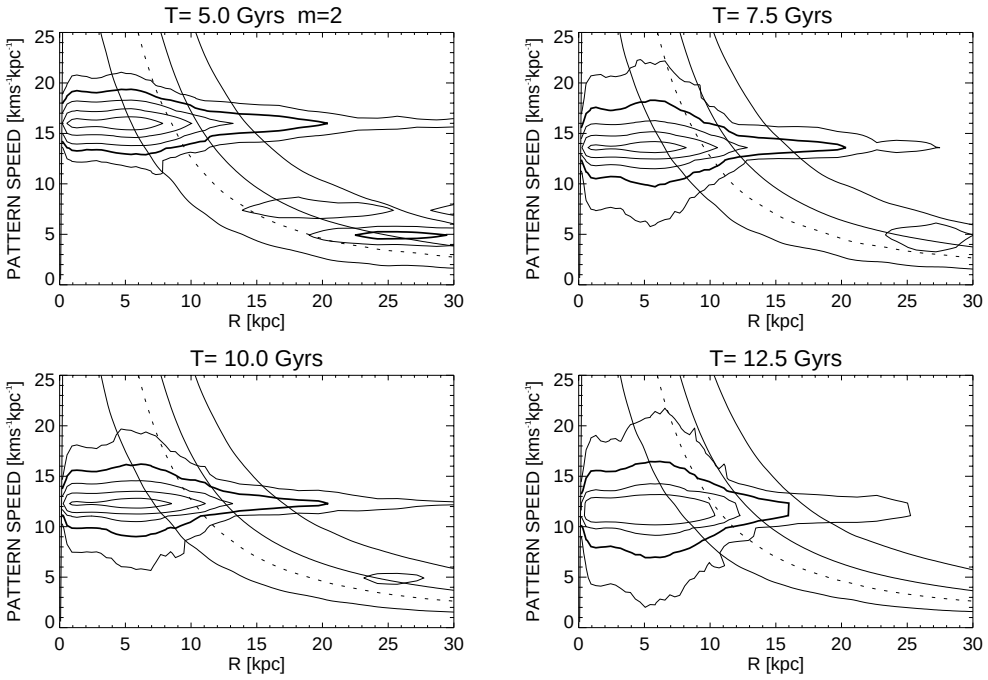

Fig. 5. The amplitude spectra of Model II. The contour levels are the same as in Fig. 3.

some models (e.g. Model I, except with twice the standard softening parameter) the patterns speed of the nuclear bar decreases rapidly after the formation of the main bar until it stabilizes, in other models (e.g. both of the models shown here) the pattern speed is not affected by the main bar.

Fig. 7 shows the evolution of Model IV. In this model the initial mass distribution is the same as in Model I, but the central parts are hotter. This is done by changing the Toomre parameter smoothly from 3.0 to 1.5 within the innermost 4.5 kpc, beyond which it has the same constant value as in Model I. This delays the formation of the main bar, and when it forms, it is longer and its pattern speed is about 16% lower. This is in accordance with Athanassoula and Sellwood (1986) who found that the growth rate of the bar modes correlates strongly with the central value of $Q_{\rm T}$ but only weakly with the value in the outer disk. The nonequality of the pattern speeds of the nuclear and the main bars is clearly demonstrated by the changes in the relative position angle (Fig. 11). The closest of the resonance overlappings are the several CR – 4/1 ones, the CR – ILR between the nuclear bar and the spiral mode S3 and the CR – OLR between the main bar and S9. What is very significant, there seems to be no resonance overlappings between the nuclear and the main bar.

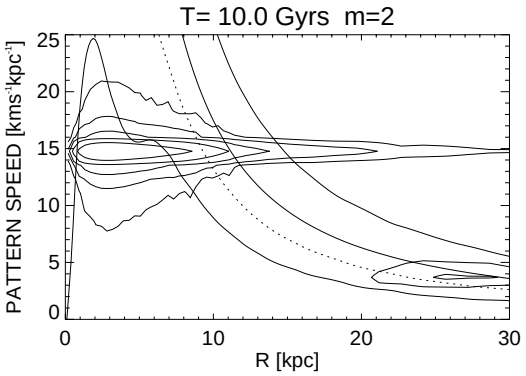

Fig. 6. The amplitude spectrum of Model III at $T = 10.0$ Gyrs. The contour levels are the same as in Fig. 3.

Table 5. The $m = 2$ modes, their resonance radii and maximum amplitudes in Model IV for different time intervals. NB refers to the nuclear bar.

T	Mode	Ω_p	$r_{\rm ILR}$	$r_{4/1}$	$r_{\rm CR}$	$r_{\rm OLR}$	$A_{\rm max}$
7.5	NB	71.3	0.9	2.1	3.3	5.5	0.27
	S1	44.7	1.7	3.3	5.2	8.1	0.11
	B	30.3	2.4	4.9	7.4	11.2	0.12
	S2	22.3	3.0	6.7	9.7	14.3	0.026
	S3	19.7	3.4	7.6	10.8	15.8	0.040
	S4	16.0	4.3	9.3	12.7	18.5	0.045
	S5	12.5	6.0	11.3	15.4	22.7	0.056
10.0	NB	71.2	1.0	2.2	3.3	5.4	0.15
	B	28.3	2.6	5.4	7.7	11.7	0.47
	S3	19.7	3.5	7.7	10.5	16.1	0.042
	S6	18.4	3.7	7.9	11.3	17.1	0.045
	S7	14.8	4.9	9.5	13.4	19.7	0.063
	S8	7.4	10.1	17.5	23.9	36.0	0.15
12.5	NB	72.6	0.9	2.2	3.2	5.3	0.12
	B	27.2	2.6	5.7	8.0	12.0	0.62
	S3	19.7	3.6	7.7	10.4	16.1	0.038
	S9	17.3	4.1	8.5	11.6	17.8	0.043
	S10	8.7	8.6	15.2	20.9	31.1	0.072
	S8	7.5	10.0	17.4	23.4	35.5	0.13

Another simulation with a nuclear bar, Model V, is shown Fig. 9. This model differs from Model I so that its bulge is formed by two parts each having half of the mass of the bulge in Model I. The particle number N is larger, 500, 000, to give better resolution. The scale lengths of the bulge components are 600 and 300 pc. Norman et al. (1996) also used combination of two Plummer bulges, but the other of their bulges had variable scale length mimicking gas flow to the center. In this model we are interested in the effect of pre-existing central mass concentration. The model developes a complex nuclear structure. First there seems to be a nuclear spiral (not discernable in Fig. 9). Then it evolves to a nuclear bar or an elongated nuclear ring. At about $T = 7.5$ Gyrs a small bar forms. It is considerably weaker than the bar in the previous models. At some stages (see Table 6), there are altogether eight modes present in the disk. Thus, there is a complicated network of possible resonance overlappings.

Table 6. The $m = 2$ modes, their resonance radii and maximum amplitudes in Model V for different time intervals.

T	Mode	Ω_p	$r_{\rm ILR}$	$r_{4/1}$	$r_{\rm CR}$	$r_{\rm OLR}$	$A_{\rm max}$
7.5	NB1	150.7		1.2	1.7	2.7	0.090
	NB2	110.9	0.8	1.5	2.2	3.6	0.34
	B	63.2	1.5	2.6	3.7	5.9	0.20
	S1	27.1	2.9	5.5	8.1	12.2	0.36
	S2	17.3	4.4	8.4	11.9	17.8	0.12
10.0	NB1	149.0		1.2	1.7	2.7	0.10
	NB2	113.5	0.8	1.5	2.2	3.5	0.18
	B	59.1	1.5	2.8	4.0	6.2	0.14
	S3	49.2	1.7	3.2	4.7	7.3	0.018
	S4	40.6	2.0	3.9	5.6	8.8	0.012
	S1	25.8	3.0	5.9	8.3	12.7	0.43
	S2	17.1	4.7	8.3	11.9	17.8	0.16
	S5	12.2	6.3	11.4	15.6	23.1	0.2
12.5	NB1	150.5		1.2	1.7	2.7	0.059
	NB2	115.7	0.7	1.5	2.1	3.4	0.13
	B1	53.1	1.6	3.0	4.4	6.8	0.24
	B2	50.5	1.7	3.2	4.6	7.0	0.29
	S1	25.2	3.2	5.8	8.3	13.0	0.27
	S2	17.2	4.7	8.2	11.8	17.6	0.25
	S5	12.3	6.2	11.1	15.6	23.0	0.14

Most of these are probably coincidental due to large number of modes. Some of the modes apparently have multiple resonance overlappings. The overlappings include OLR – CR, CR – 4/1 and CR – ILR. At $T = 12.5$ Gyrs, two close modes are seen in the amplitude spectrum, marked as B1 and B2 in Table 6. These are not really two different bar modes: the pattern speed of the bar changes so that it gives this impression. The $m = 4$ amplitude spectra, which can be calculated using a smaller time interval due to higher resolution, clearly show that there is only one mode present.

These models are just two examples of our simulations exhibiting nuclear bars. For example, in a simulation whose initial state was the same as in Model I except that the Toomre's $Q_{\rm T}$-parameter was 2 throughout the disk, a nuclear bar formed before the main bar. Although Friedli & Martinet (1993) found that the presense of massive dissipative component was needed for the formation of the nuclear bar, we did not find that necessary. Also the formation of the nuclear bar before the main bar is something that did not happen in Friedli and Martinet's simulations.

3.2. Evidence of mode coupling

According to Masset & Tagger (1997) the presence of non- linear mode coupling should be evident from the amplitudes of the beat modes. In the case of normal beat modes, their amplitudes should be proportional to the product of the amplitudes of parent modes. When the process of non-linear coupling is present, the beat modes are expected to be boosted, having peaks near the area of resonance overlapping. In the case of two $m = 2$ modes, assumed to be in CR – ILR coupling, $m = 0$ and $m = 4$ beat

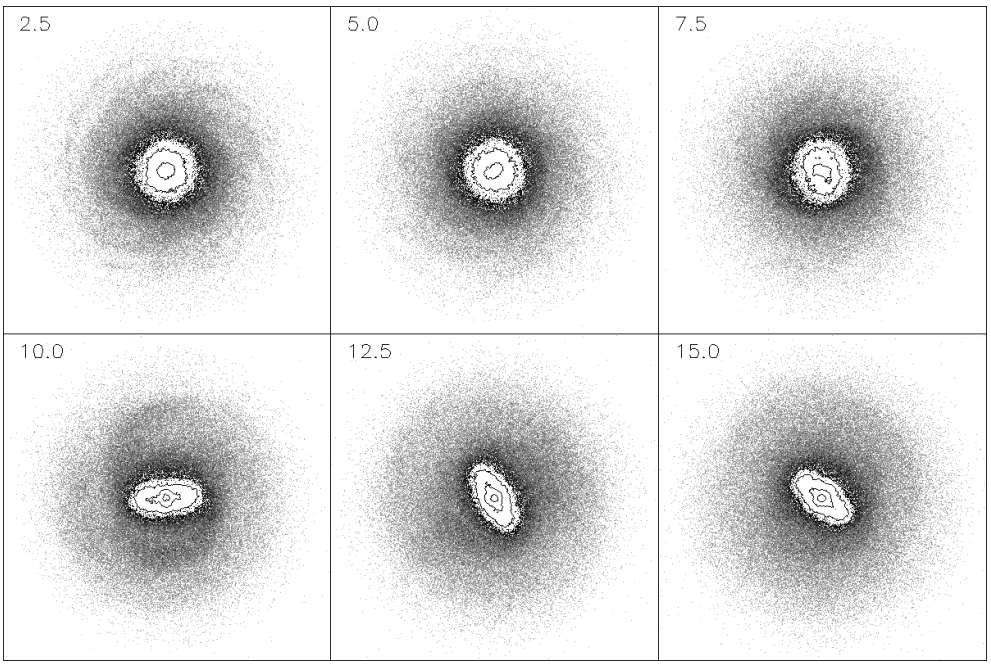

Fig. 7. The Evolution of Model IV.

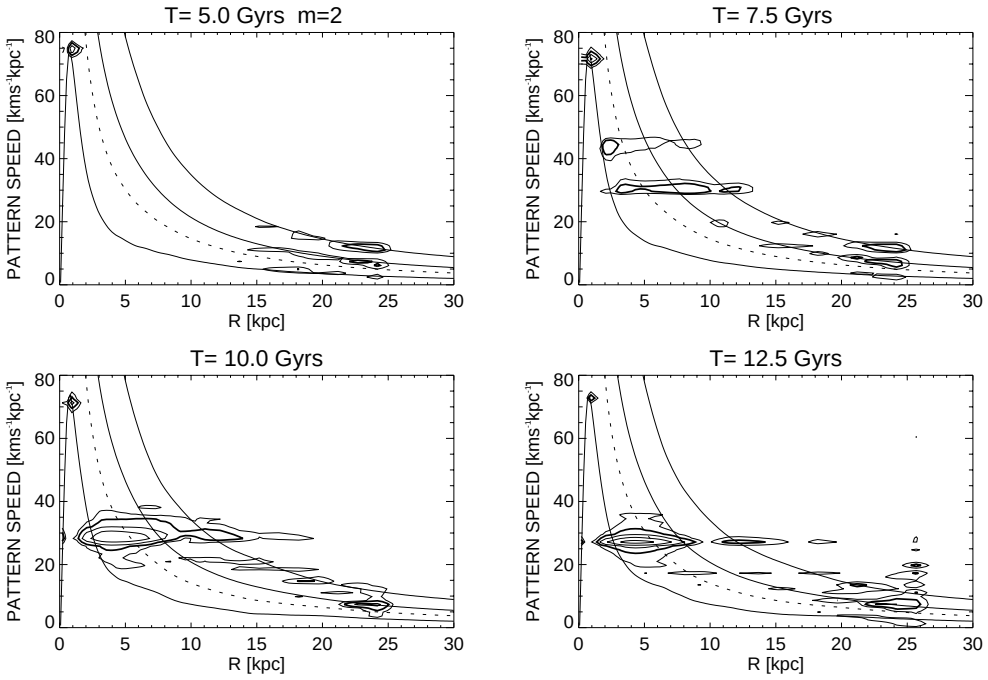

Fig. 8. The amplitude spectra of Model IV. The contour levels are the same as in Fig. 3.

modes would be produced. Fig. 12 shows $m = 0$ and $m = 4$ spectra of Model I, by $T = 12.5$ Gyrs. The predicted beat modes of couplings between the bar and the modes S2 and S3 (see Table 2) are clearly present. The wave frequencies of the $m = 0$ beat modes, calculated from the first part of Eq. 6, are 44.2 and 33.4 kms^{-1}kpc^{-1} (B – S3, B – S2). The pattern speeds of the $m = 4$ beat modes are 23.7 and 21 kms^{-1}kpc^{-1}. In Fig. 13 we show some of these products and the observed amplitudes of the beat modes in these models. As we can see, in Model I, both B – S2 and B – S3 behave in a similar way. In the inner parts, the amplitude profile of the beat wave is more or less what is expected for a non-coupled case, but deviates strongly near the resonance overlapping area, reaching peak between its ILR and CR. This suggests that both of the spiral modes are actually in CR – ILR coupling with the bar. As an additional example in Fig. 13, there is a clear CR – ILR coupling between bar and S10 in Model IV by $T = 12.5$ Gyrs.

What happens to the CR – 4/1 couplings between different modes, the situation is less clear. The $m = 0$ and $m = 4$ beat modes of the $m = 2$ components show no unambiguous signs of being boosted above normal level. Because the $m = 4$ ILR of one mode overlaps the corotation of the other mode, one

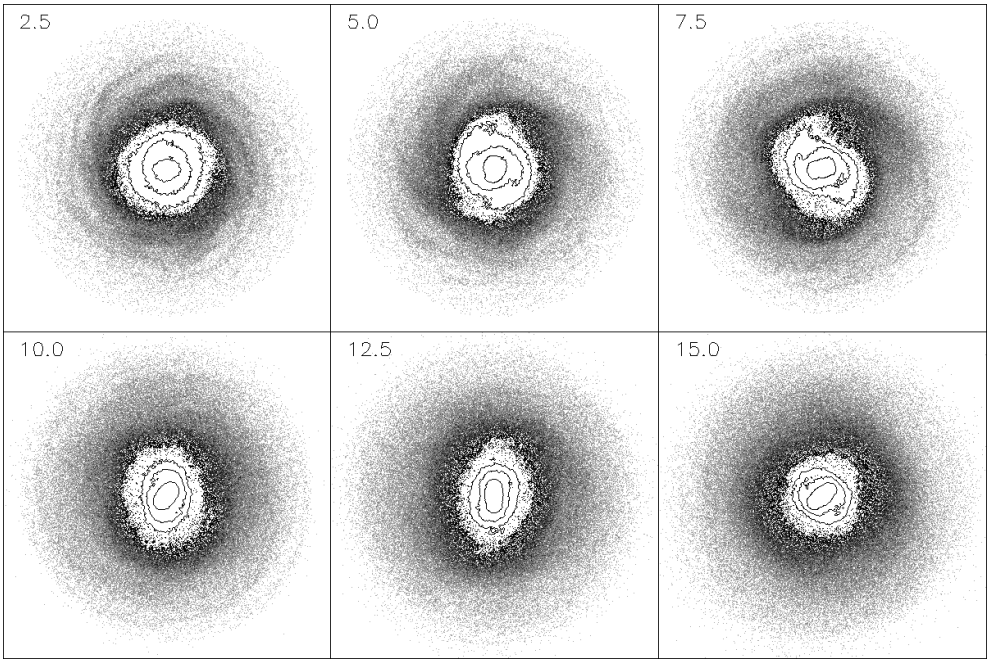

Fig. 9. The Evolution of Model V.

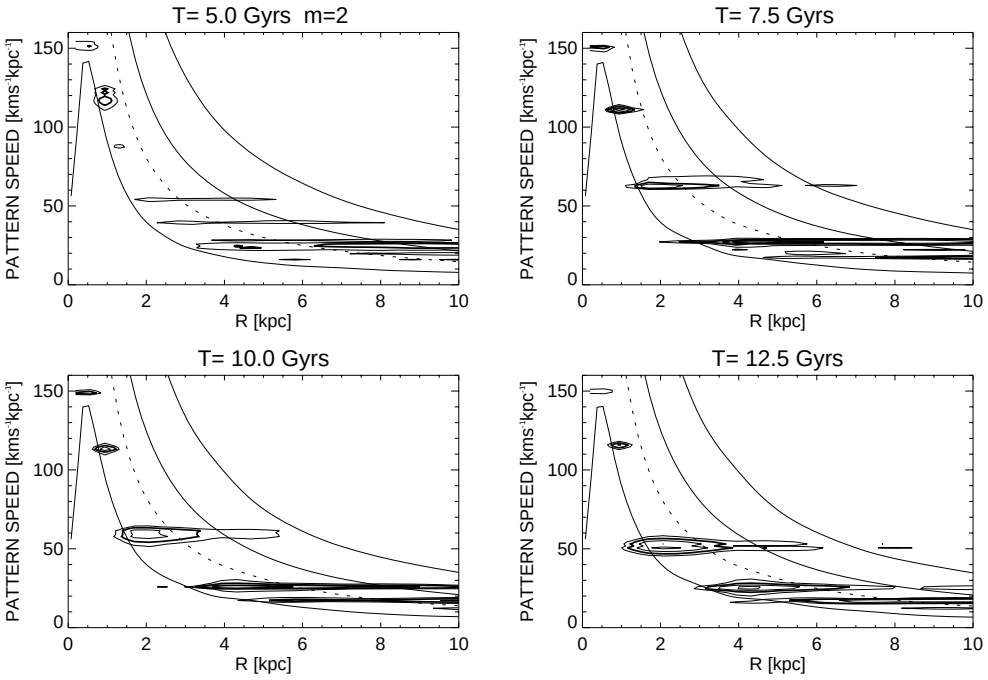

Fig. 10. The amplitude spectra of Model V. The contour levels are the same as in Fig. 3. Note that only the inner parts are shown.

could also expect $m = 2$ and $m = 6$ beat modes to be present. However, they are usually not found or they are so weak, that there is probably no coupling. A possible exception is the mode S4 in Model I, which could be the $m = 2$ beat mode of the $m = 4$ component of S3 and the $m = 2$ component of S2. However, there was no $m = 6$ beat mode of the suspected coupling.

In models II and III the beat modes are hard to find, probably because in the area were the parent modes overlap, their amplitudes are so weak that the resulting beat modes, even if present, do not rise over the noise level. One possible example is shown in Fig. 13, OLR – ILR overlapping of the bar and the mode S2 in Model II, $T = 5$ Gyrs. The $m = 4$ beat mode shows a peak slightly outside the radius where the resonances overlap. If this coupling is real, it is of different type from that demonstrated by Masset and Tagger. Another example of apparent coupling variations is the OLR – CR coupling between the bar and the mode S9 in Model IV, $T = 12.5$ Gyrs. In this case the peak amplitude is slightly inside the overlap area, between the CR and the OLR of the beat mode.

We have also tried to check what is the role of $m = 1$ and $m = 3$ modes in these models. For the coupling of $m = 1$, $m = 2$ and $m = 3$ modes with equal pattern speeds (as

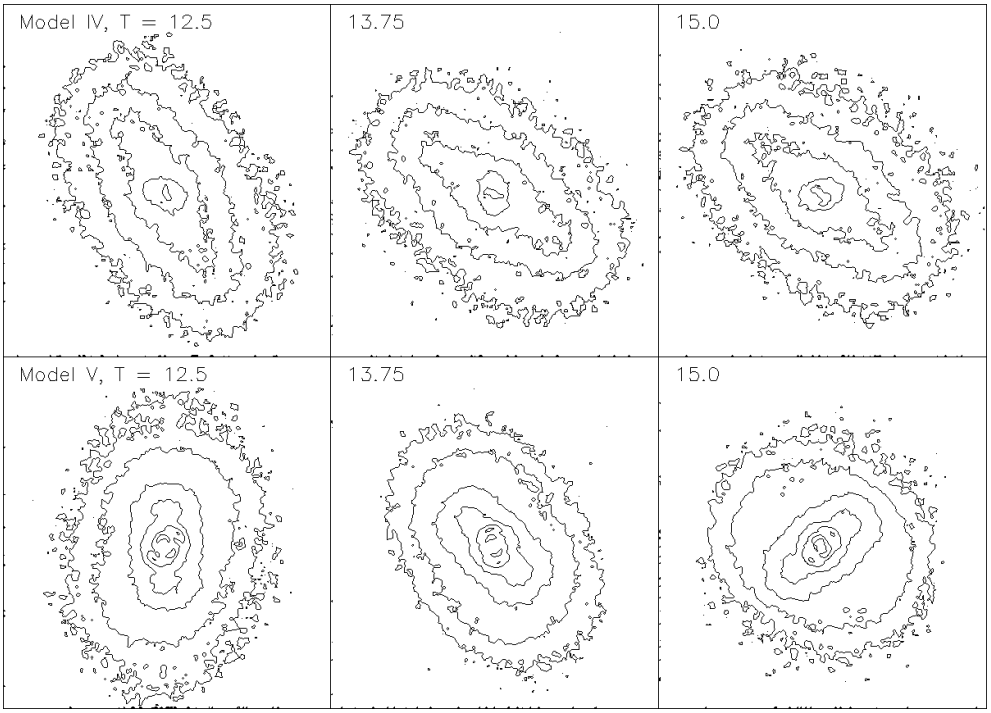

Fig. 11. Zoomed images of the nuclear parts in models IV and V. The horizontal width of the frames is 10 kpc. At least in Model V, there are three different bar components present, with clearly different pattern speeds.

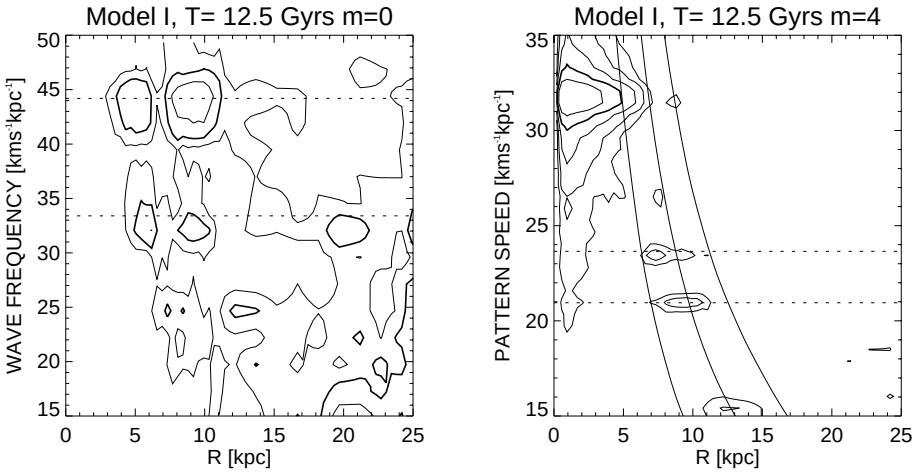

Fig. 12. The $m = 0$ and $m = 4$ amplitude spectra of Model I at $T = 12.5$ Gyrs. The contour levels for $m = 0$ spectrum are 0.0025, 0.005,0.01 (drawn with a thicker line) and 0.02 and for $m = 4$ spectrum they are 0.01, 0.02 (drawn with a thicker line), 0.04, 0.08 and 0,16. The predicted beat mode pattern speeds of B – S2 and B – S3 couplings are shown as dotted lines. Ω and $\Omega \pm \kappa/4$ curves are shown as continuous lines. Note that features at the $m = 4$ spectrum with pattern speeds of 32.0 and 15.3 kms^{-1}kpc^{-1} are connected to principally $m = 2$ modes.

suggested by Elmegreen et al. 1992a) we did not find any clear evidence. The bars seem to be very symmetrical, so they do not have significant $m = 1$ or $m = 3$ components. The situation is different with some of the spiral modes. For example, in Model I ($T = 12.5$ Gyrs the $m = 1$ amplitude of mode S3 is about 0.05, clearly above the noise level, but considerably less than the $m = 2$ amplitude. In addition to cases, where basically $m = 2$ modes have also odd components, there are also genuine $m = 1$ or $m = 3$ features in the amplitude spectra, but these are considerably weaker than the two-fold modes. Usually, we could not find beat modes of possible couplings between the odd modes and the $m = 2$ mode, which is not surprising because the predicted amplitudes are so low. The only clear exception is shown in the last frame of Fig. 13, which shows the $m = 5$ and $m = 1$ beat modes of the OLR – ILR coupling between the bar and $m = 3$ mode with pattern speed 11.5 kms^{-1}kpc^{-1} in Model I, $T = 10$ Gyrs. Both of the beat modes have a peak near the resonance overlapping radius. One should note that the $m = 1$ beat mode is retrograde, and its peak is located in the radius where the pattern speed is equal to $\Omega - 2\kappa$. This also coincides with the resonance overlapping.

3.3. The effect of different model parameters

The five cases presented in detail were chosen to show different situations in relation to pattern speeds and so do not form a systematic sequence. However, during the survey, we made several simulation subseries on the effect of various model parameters. In this subsection we present shortly the dependencies we observed. Most of our models form bars. Only systems with a dominating halo and/or a very hot initial disk can escape this. This agrees well with the previous studies on bar forma-

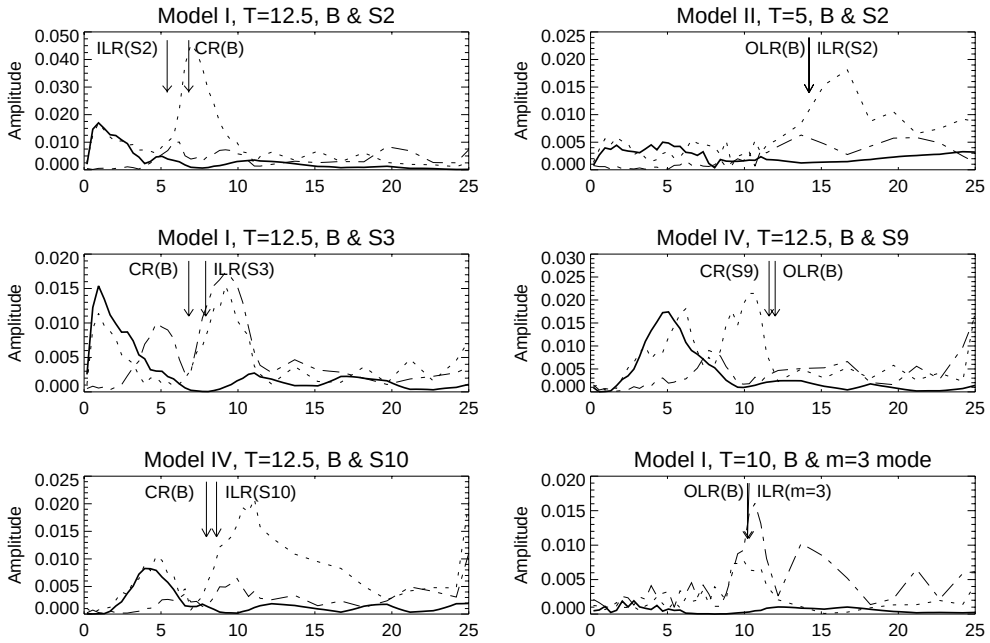

Fig. 13. Examples of boosted beat modes in our models. The products of the amplitudes of the parent modes are shown as continuous lines. In the first five cases the amplitudes of $m = 4$ beat modes are drawn with dotted and $m = 0$ modes with dot-dashed line. In the sixth case, these linestyles are used for $m = 5$ and $m = 1$ modes. The arrows show the selected resonance radii of the parent modes.

tion (see e.g. Ostriker & Peebles 1973). In models with a very strongly concentrated bulge or a high Toomre parameter, the bar formation was delayed so much that it can take more than 10 gigayears to have a main bar component. An extreme case of this was achieved when the scale length of the bulge was reduced to 300 pc, other parameters being like in Model I: no bar component was formed during the 15 gigayears of the simulation. Interestingly, the spiral amplitudes were about as strong as in Model I, and are present throughout the simulation. However, one should note that the pattern speeds of the modes are different from those in Model I. There are several modes present, just as in Model V that also has a massive central concentration. The resonance overlappings include four OLR – CR, two CR – 4/1 and a CR – ILR overlappings. Some of the mode pairs have double overlappings. This model seems to indicate that the bar cannot be crucial for the formation of the outer spiral structures and that the mode couplings could rather modify the independently formed modes of the outer disk. This contrasts with Masset & Tagger's (1997) results, where the inhibition of bar formation also dramatically suppressed the outer spiral modes.

Shapes of the bars in our simulations vary from elliptical or boxy to systems where the bar is narrowest near its center, thus giving a dumbbell appearance. Sometimes there are narrow arcs outside the main body of the main bar. These forms might correspond the so called ansae that are seen in many early type galaxies. Thus the ansae could be stellar dynamical features as suggested by Buta (1996).

The formation of the bar induces strong noncircular velocities and the rotation curves measured in different azimuthal directions can differ considerably (see e.g. Duval & Athanassoula 1983). Therefore, we use axisymmetrical rotation curves, which are calculated from the radial force. These curves show clearly the effect of the bar: when the bar forms, the peak of the azimuthally averaged rotation curve rises and beyond the end of the bar, the rotation velocity becomes lower than the initial value. These changes are strongest in the disk dominated systems, especially in Model III, in which the rotation curve becomes considerably steeper.

The effect of the softening parameter ϵ was tested by running Model I with values 187.5, 375 and 750 pc ($\epsilon = 1/16, 1/8$ and $1/4\ R_{\rm d}$). With the reduced ϵ, the bar forms faster and is shorter and its pattern speed is lower than in the other two cases. Resonance overlappings (CR – ILR, CR – 4/1) are also present but the slower modes disappear by 10 Gyrs. In the simulation with largest ϵ, the main bar forms after 10 Gyrs. There are several modes in this simulation, e.g. a nuclear bar that forms before the main bar.

In the initial stage the outer truncation of the disk is usually 9 scale lengths, although we have made some simulations with truncation at 6 and 3 scale lengths, otherwise being similar to Model I. The models with truncations at 9 and 6 scale lengths are practically identical, no essential difference in their evolution was found. On the other hand, the strongly truncated disk behaves very differently. Its bar has a different shape without a dumbbell-form. The pattern speed of the bar is higher and there are only two rather weak slower modes. With the main bar they form a chain of CR – 4/1 overlappings. The pattern speed effect is probably explained by having less interaction between the bar and the outer disk. Combes & Elmegreen (1993) used even more strongly truncated disks but that is probably not realistic.

The initial pattern speed of the bar seems to be determined by the degree of central concentration of the bulge so that more concentrated models have faster bars. This is in agreement with Sellwood's simulations (1981), but one should note that this result fits to disk and halo dominated systems separately: models with more or less similar inner rotation curves (e.g. models I and II), but large differences in halo contributions, can have dramatically different bar pattern speeds. In models with larger bulge

Table 7. Bar pattern speeds and maximum amplitudes in simulations with different particle numbers N, determined at $T = 12.5$ Gyrs.

N	$\Omega_{\rm bar}$	$A_{\rm bar}$
32 000	39.4	0.54
80 000	32.0	0.68
200 000	32.0	0.93
500 000	32.0	1.07
1 250 000	30.8	1.04

scale lengths, the number of the present modes is smaller than in Model I. In most occasions they do not have clear resonance overlappings.

In all models the pattern speeds of the bar components are declining, but usually this decline slows down considerably during the first few gigayears after the bar formation. One should also note that this often happens while the pattern speeds of the spiral modes remain constant. According to Sellwood (1981), the bar slow down process is accompanied by the growth of the bar. We found it difficult to measure the bar lengths from isodensity contours or surface density plots. Instead we use the phase angles of maximum density as found in the Fourier decomposition. Phase angles are roughly along the bar until very near the corotation, although there is evident twisting starting by the inner $4/1$ -resonance. We estimate that the error marginal in the definitions of bar length is rather large, about 10%. Martin (1995) gives the same estimated accuracy in his study on lengths and axial ratios of the observed bars.

We have measured the relation $\mathcal{R} = r_{\rm CR}/r_{\rm bar}$ for several of our models. The extremes are 1.0 and 1.3, while most of the values are between 1.1 and 1.2. This relation stays more or less constant during the simulation, and so the bar follows similar growth process as noticed by Sellwood (1981). It is possible that in real galaxies the interaction with halo particles may slow down the bar rotation rate so much that the bar cannot grow fast enough to reach the corotation (Little & Carlberg 1991; Debattista & Sellwood 1997). This is one explanation why the most favoured value seems to be $\mathcal{R} \approx 1.2$ (see e.g. Elmegreen 1996). Another possibility is the lack of bar supporting orbits beyond the inner 4/1-resonance (Patsis et al. 1997).

Also the effect of two simulation method related parameters, the particle number and the grid geometry, was tested. The Model I simulation was repeated by several particle numbers N between 32 000 and 1.25 million (the particle number was multiplied by 2.5 between two successive simulations). The pattern speeds and the amplitudes of bars in simulations with different N are listed in Table 7. The bar in 32 K model rotates faster, apparently due to reduced interaction with the sparsely populated outer disk. The pattern speed differences in other models are not significant, whereas the bar strength seems to grow with particle number. The evolution of the $Q_{\rm T}$ -parameter is very similar in all these simulations, so the heating of the disk is not due to two-body relaxation effects.

The amplitude spectra of Model I variants with different N are shown in Fig. 14. The trend is that the slower modes get stronger when the particle number is increased. This keeps the chain of CR – 4/1 overlappings unbroken to the end of the simulation. This behaviour is different from Masset & Tagger's (1997) model where doubling the particle number (from 80 000 to 160 000) weakened the intermediate mode. We have also run Model II with 1.25 million particles. As in the case of Model I, the increase of N strengthens the modes which rotate slower than the bar. However, the bar mode still dominates even beyond its OLR.

The effect of the grid geometry was tested by reproducing Model I simulation using a cartesian grid. When the resolution of this grid was high enough, e.g. 256×256 with cell width 375 pc, there was no essential difference. However, the situation changed when twice coarser cartesian grid was used: the bar was longer, its pattern speed was lower, its shape was different and the system had a strong nuclear mode. Very similar behaviour was seen when the resolution of the logarithmic polar grid was reduced to a corresponding level.

We have also tested the effect of the length of the time step by reproducing some simulations with shorter time steps (0.5 and 0.25 times the original one). Neglecting extreme cases, the differences are small. Especially, the nuclear bars of Fig. 11 were still obtained with smaller time steps, showing that they cannot be artefacts due to integration inaccuracies. The pattern speeds are approximately the same in simulations with different time steps, but on few occasions the relative strengths of the modes can be slightly different.

3.4. Shapes of the modes

We have used Fourier decompositions of the disk surface density to study the short term evolution of the system. The animations show that in the presence of several modes, the morphology can change quickly, e.g. from a situation clearly showing the domains of different modes (structure within structure) to a mirage of a two-armed grand design structure throughout the disk. Somewhat similar behaviour is demonstrated by Lin & Low (1990, Fig. 1).

We have reconstructed the shapes of the modes with the method described in Sect. 2. Fig. 15 shows the results for 1.25 million particle version of Model I. Mode B has a clear bar shape with weak spiral outside the bar. S2 and S3 are clearly spiral shaped and show amplitude modulations. One should note that this method shows how the the B-mode can have a bar shape slightly beyond the corotation radius calculated from the linear approximation. The mode reconstruction gave basically similar shapes for the modes in the other simulations. The only other example we show is that of Model II, shown in Fig. 16. This clearly indicates how the whole disk is dominated by one mode, which has a bar shape in the inner parts and a trailing spiral shape in the outer parts. Amplitude modulations are not seen in this mode.

3.5. Gas morphology

We have also added gas component in the form of uniformly distributed (inside 9 scale lengths) dissipative test particles to some

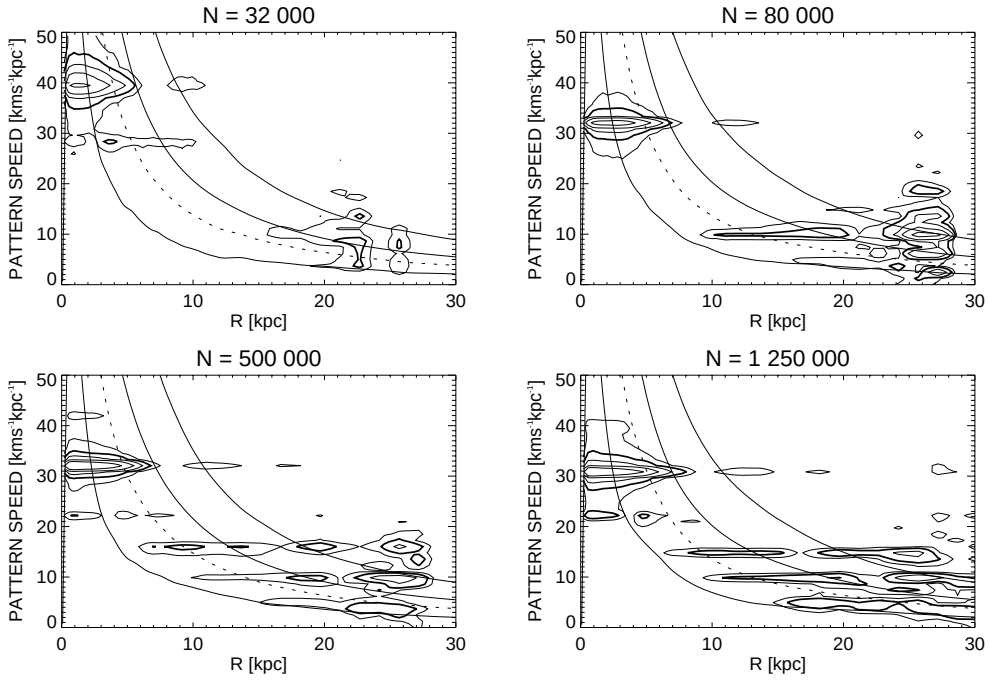

Fig. 14. Comparison of amplitude spectra of models with different N for $T = 12.5$ Gyrs.

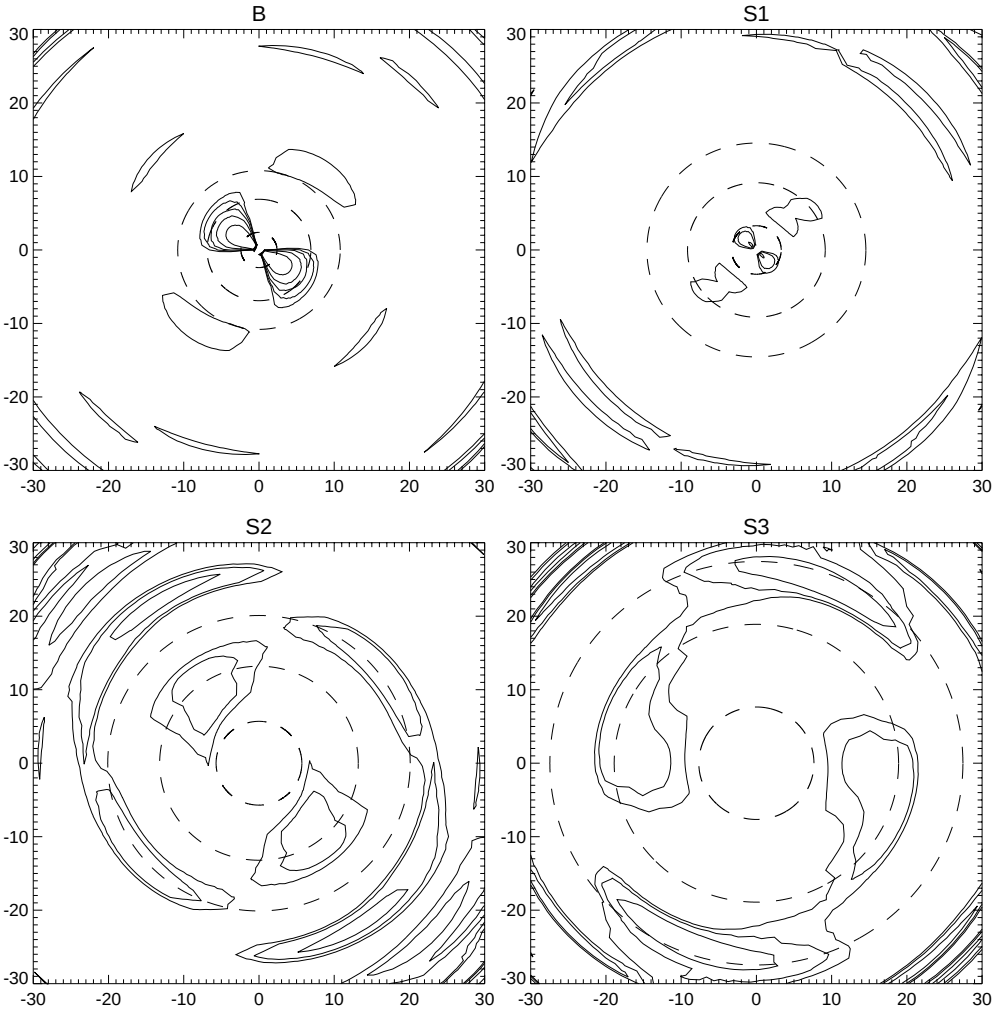

Fig. 15. Shapes of the individual modes in the 1.25 million particle version of Model I, $T = 12.5$ Gyrs. The contour levels are the same as in Fig. 3 and correspond the perturbed density due to $m = 2, 4$ components. The radii of corotation and inner and outer Lindblad resonances are shown as dashed lines.

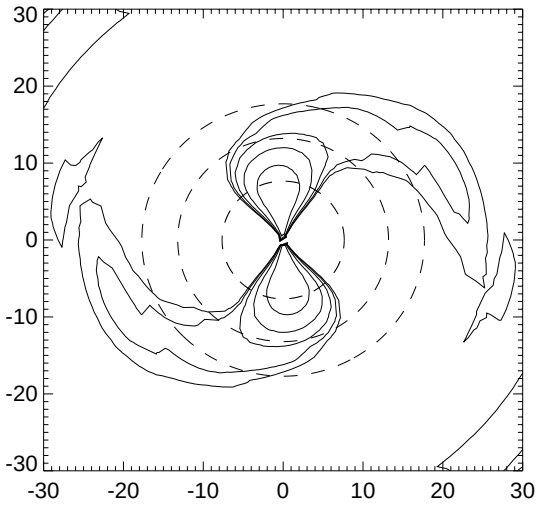

Fig. 16. The shape of the dominant mode in Model II. The resonance radii are indicated as in Fig. 15.

of our simulations. The evolution of gas component in models I – II, IV – V is shown in Fig. 17. Because the test particles are massless they follow the potential due to stellar distribution. The features are sharper in gas component. Due to its dissipative nature the gas response lags and the gas component can gain or lose angular momentum.

In Model I the gas component forms two parts with different morphologies. In the inner area, inside the OLR of the bar, the gas features are corotating with the bar. Most notable detail is the inner ring surrounding the bar. The outer structure consists of several tightly wound spiral arms. The inner edge of this structure resembles outer pseudorings but does not easily fit to the observed categories of Buta (1995).

The gas morphology of models II and III is so similar that only Model II is plotted. In the earlier stages both show corotating two armed spiral structure starting from the end of the bar, but the radial flow is so strong that most of the gas particles end up either to the nucleus or to the outer part forming a multiarmed figure.

Model IV has a beautiful nuclear ring that forms before the main bar. However it seems to become perpendicular to the main bar although there is a nuclear bar with a higher pattern speed inside the nuclear ring, which in principle might distort its orientation. This model has an inner ring displaying more complicated structure than that in Model I. The spiral arms seem to form an outer pseudoring, however its shape is changing and the classification is uncertain.

Model V has many different pattern speeds in its stellar component and hence its gas morphology is very complicated. The innermost ring is a nuclear ring (actually a double nuclear ring but the resolution of the figure is not high enough). Although it is in the area affected by both the nuclear and main bar components its orientation with respect to the main bar is almost constant, only small swinging motion is seen. However, there are other simulations where the orientation of the nuclear ring changes constantly, following the nuclear bar. The orbits of the gas particles forming such ring are probably of the type studied by Maciejewski & Sparke (1997). Similarly behaving nuclear ring was also present in the simulations of Friedli & Martinet (1993) but in their case the nuclear bar is destroyed and the nuclear ring eventually became perpendicular to the bar. The next ring in Model V is the inner ring of the main bar component. After that comes a ring that is in the distance where one would expect the outer ring of the main bar to be. However, this is not an outer ring in this sense: its shape and orientation with regard to the main bar are changing constantly. The reason for this is that the ring is affected by two modes with different pattern speeds. In addition to previously discussed features, the outermost spiral structure seems to form a pseudoring.

4. Discussion

We have observed several different situations in our models. There are systems where the spiral structure corotates with the bar and others where pattern speeds are different. Mode coupling is present in some simulations, especially in systems with massive halos. The existence of massive halos in the disk areas of barred galaxies has been questioned by "live halo simulations" (Debattista & Sellwood 1997) so our halo dominated models may not be realistic. The simulation that Masset & Tagger (1997) give as an example of mode coupled case has the same problem.

In addition to CR – ILR mode coupling, that seemed to dominate Masset & Tagger's (1997) simulation example, we have noticed other possibilities. The most common resonance overlapping is CR – 4/1, which sometimes forms chains of different modes. For an extreme example, in Model I, $T = 7.5$ Gyrs, there are three mode pairs having this connection! Although there is no evidence of CR – 4/1 coupling as boosted beat modes, this overlapping is so common that we consider unlikely that it is totally random, i.e. it is related to some physical process.

Masset and Tagger's simulation also had an intermediate mode with pattern speed between the pattern speeds of the bar and the coupled spiral mode. They suggested that this intermediate mode could be the subharmonic of the $m = 4$ beat wave or in OLR – CR coupling with the bar. The latter explanation could be true for one of the modes in Model I (S1) but neither can be true for S2 which amplitude is initially higher than that of the suspected CR – ILR coupled mode. One explanation could be that the bar can feed two modes via CR – ILR coupling, one with its ILR inside bar's CR and another with ILR outside it. Although this resonance overlapping is quite distant (the difference in resonance radii is about 20%), the presence of boosted beat modes between the bar and both of the spiral modes supports mode coupling. Also in Model IV, there is a clear CR – ILR mode coupling between the bar and one of the spiral modes.

Besides the previously discussed mode couplings, other resonance overlappings are also observed, some of which can be purely incidental. The cases where we found further support by peaked beat modes are OLR – ILR coupling and CR – OLR cou-

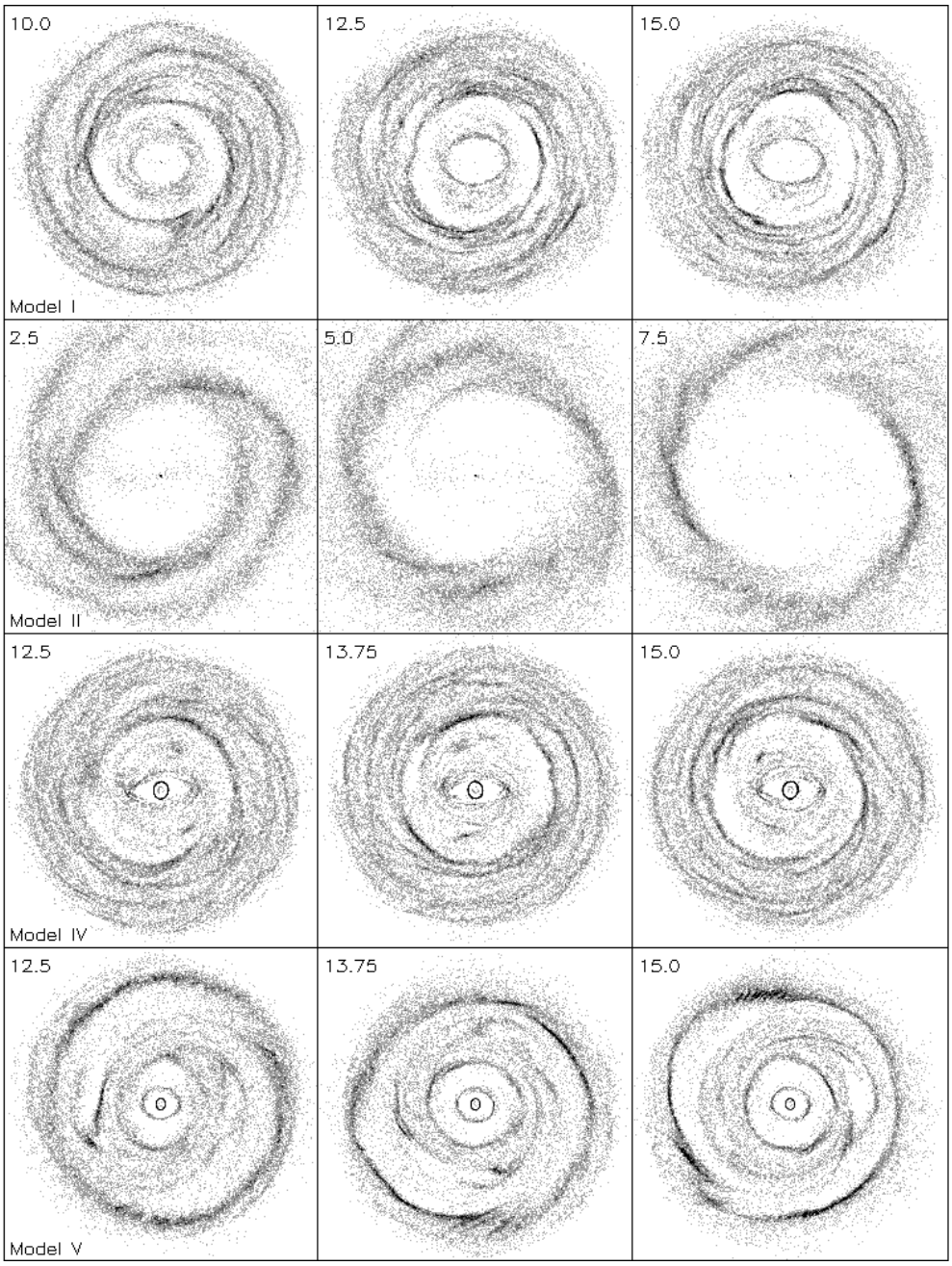

Fig. 17. The evolution of the gas component in models I-II and IV-V. The particle positions are rotated so that the bar is horizontal. The width of the frames is 18 disk scale lengths.

pling between $m = 2$ modes, and OLR – ILR coupling between $m = 2$ and $m = 3$ modes. In at least one simulation, there was a temporary double overlapping between two modes (CR – 4/1 and OLR – CR). Some simulations, e.g. Model III, had multiple pattern speeds without any obvious resonance overlappings between major modes. Furthermore, we did not find any clear evidence of mode coupling process involving $m = 1$ or $m = 3$ modes with same pattern speeds, as suggested by Elmegreen et al. (1992a).

The simulations cover the evolution for about one Hubble time and different stages can be determined according to which modes are dominating in the disk. For example, it takes several gigayears to reach strong mode coupling. This also means that strictly speaking our models are valid only for genuinely isolated galaxies. It has been shown that encounters can provoke bar formation (e.g. Noguchi 1987, 1996; Salo 1991) but their effect on the evolution of a multi patterned system is not clear and should be studied. According to Elmegreen et al. (1992b) the interactions can destroy outer rings and in M 51 -type systems they can be responsible for most of the observed spiral structure (Toomre & Toomre 1972; Salo & Laurikainen 1993).

Outer ring structures and their resemblance with bar related periodic orbits near OLR has been considered a strong evidence for corotating bar and spiral structures. On the other hand it has been suggested that these rings could be transient features (Sellwood &Wilkinson 1993). The strength of the resonance expla-

nation weakens when we consider that there are several strongly barred galaxies without these rings. An explanation could be that the timescale for outer ring formation is relatively long, several gigayears, or depends on the gas distribution. Another possibility is that the formation of resonance rings is inhibited by additional non-corotating spiral modes.

In these simulations the explanation based on long time scale is at least partly valid. The outer rings we get (mainly in the gas component), form in timescales of more than one gigayear. What comes to pattern speeds, outer rings habit areas where two patterns may be present. In simulations where a strong pattern with lower frequency is present, the morphology does not resemble R_1 outer rings (which major axis is perpendicular to the bar, see e.g. Buta & Crocker 1991) and is more open resembling sometimes R'_2 pseudorings (which major axis is parallel to the bar). However, on most occasions the shape does not fit Buta's outer ring morhologies. The formation of outer rings, especially of the R_1-type, thus most probably requires that the inner pattern is clearly stronger than the outer one in the vicinity of OLR. This means that N-body models are quite different from test particle simulations (e.g. Schwarz 1981; Byrd et al. 1994). It is clear that the latter type of simulations with analytical potentials with just one pattern speed present may overestimate the efficiency of the ring formation process.

A very interesting feature in the gas component of models II and III is that the two armed structure starting from the ends of the bar corotates with the bar whereas the multi-armed shape marks the area where lower mode becomes considerable. This is in accordance with the results of Elmegreen & Elmegreen (1995), who found that the size of the bar correlates with the size of the domain of the two-armed part of galaxies. It seems that the radius where two-armed phase ends is roughly twice the half length of the bar. Outside this area, galaxies often have multi-armed structure. The radius where the two armed spiral ends can be interpreted as the outer limit of the corotating spiral. In systems dominated by one mode this should happen near OLR. However, when other modes are present, this could happen even closer to the ends of the bar. Some systems have different spiral structures: inner and outer ones. When there are several modes present at the same radius, the structure can be very complicated, even incoherent. An example of this could be the outer disk of Model I. Such a situation was anticipated by Sygnet et al. (1988).

Examples of real multi-patterned galaxies could be NGC 1068 and NGC 1566 (Bosma 1992). Both of these galaxies have spiral structures in different radial scales. Another interesting case is NGC 1398. Moore & Gottesman (1995) tried several models to fit the observed morphological features with specific resonances. They got best fit when the spiral structure (or in this case the outer spiral) had a lower pattern speed than the bar so that there was a resonance overlapping in the sense that the corotation of the spiral coincided with the OLR of the bar. Elmegreen & Elmegreen (1995) list this galaxy of having small bar ($R_{\rm bar}/R_{25} = 0.21$) and give the end of the two- armed phase of the spiral structure at the distance $0.33\ R_{25}$. This corresponds with the small inner spiral structure just in the vicinity of an inner ring. On the other hand Buta (1995) has classified this galaxy having a double outer pseudoring $R_1R'_2$ that is usually thought to form in the OLR of the bar. In the rectified V -band image in Moore & Gottesman (1995) one can hardly see R'_2 component; the outermost part of the spiral does not seem to form a pseudoring. If the bar reaches close to corotation as Moore and Gottesman suggest, then this could be an observed example of a galaxy with two different spiral structures resembling thus our simulations. The complicated structure near the suggested OLR of the bar (see Figs. 13 and 14 in Moore & Gottesman 1995) could be related to interaction of two modes. The gas component of Model V has two outer pseudorings, related to different modes. This is exactly what is observed in galaxy NGC 2273 (van Driel & Buta 1991). The coexistence of several modes with different pattern speeds could also explain observations of galaxies with misaligned structures like the strange system ESO 565-11 (Buta et al. 1995).

In addition to bar/spiral pattern speed multiplicity, there can be nuclear bars with higher pattern speeds than the main bars. This is strongly supported by the observations: the orientations of the nuclear bars relative to the main bars seem to be random (Friedli & Martinet 1993). If they were connected solely to the ILR of the main bar, the orientation would be nearly perpendicular. When our simulations have nuclear bars they usually form before the main bars. Examples of this kind of behaviour could be NGC 4553 and NGC 7702, both having a nuclear bar but not a clear main bar (Buta 1991; Buta & Crocker 1991). If the nuclear bar survives the formation of the main bar, it can have a CR-ILR resonance overlapping with the main bar, but not necessarily: in some of our simulations there is no clear resonance overlapping between the bar components. Unlike Friedli & Martinet (1993), we did not find the presence of massive dissipative component necessary for the formation of the nuclear bars.

5. Conclusions

Our main conclusions are as follows:

1) The relation between the bar and the spiral structure is complicated and there is probably no unique way to explain the morphology of barred spiral galaxies. The spiral arms can corotate with the bar or have a lower pattern speed. Also mixed cases where the inner part of the spiral corotates and outer part is slower may exist.

2) Although mode coupling is present in many cases, it is hardly a universal situation in barred galaxies. Often there are no evident resonance overlappings and curiously, the most usual overlapping seems to be CR – inner 4/1, not CR – ILR that has been previously proposed. Frequently there are many modes present and they can form a temporary chain of CR – inner 4/1 couplings. However, there is no further evidence for this mode coupling in the form of boosted beat modes. On the other hand, such are present in the CR – ILR, CR – OLR and OLR – ILR couplings. There is also one case with OLR – ILR coupling between $m = 2$ and $m = 3$ modes. Mode coupling seems to be strongest when halo contribution to the rotation curve is large. However, according to Debattista & Sellwood (1997) such models may not be realistic for barred galaxies.

3) The strong two-armed spirals that begin from the ends of the bar in grand design galaxies and weaker two armed structures in the central parts of multi-armed barred galaxies are probably in most cases corotating with the bar. The end of the two-armed structure may happen in the distance where the outer mode becomes so strong that no coherent pattern can exist. Galaxies with prominent outer rings are systems where one mode dominates over most of the disk and the outer patterns do not interfere too much. This might happen more easily in the galaxies with relatively large bars and OLR near the edge of the stellar disk. This is the case in our disk dominated models.
4) The existence of two or more modes may explain why many barred galaxies do not have outer rings or pseudorings. This can also explain the existence of multi-patterned galaxies. A special case of this phenomenon could be the galaxies with misaligned structures. Modeling attempts should be done for apparently multi-patterned galaxies to confirm the suspected existence of separate pattern speeds in these systems. Different pattern speeds may explain difficulties in identifying features with certain resonances and might also be responsible for some difficulties in modelling of individual galaxies.
5) Nuclear bars usually form before the main bar and they have higher pattern speeds. In some models they slow down and become part of the main bar, but there are also models where they survive for several gigayears.

For the limitations of these models (no 3D evolution, analytical halo, no self-gravitating gas component), our results are preliminary. We are going to study the generality of these conclusions by including the effect of the above mentioned processes.

Acknowledgements. The authors wish to thank the referee, Dr. M. Tagger, for most valuable comments. Financial support from the Kordelin foundation, the Väisälä Foundation, the Wihuri Foundation and the Academy of Finland is acknowledged.

References

Athanassoula E., Sellwood J.A., 1986, MNRAS 221, 213
Bertin G., Lin C.C., Lowe S.A., Thurstans R.P., 1989, ApJ 338, 78
Bosma A., 1992, In: Longo G., Capaccioli M., Busarello G. (eds.) Morphological and Physical Classification of Galaxies. Dordrecht, Kluwer, 207
Buta R., 1991, ApJ 370, 130
Buta R., 1995, ApJS 96, 39
Buta R., 1996, In: Buta R., Crocker D.A., Elmegreen B.G. (eds.) Barred Galaxies. IAU Colloquium 157, ASP, San Francisco, p. 11
Buta R., Crocker D.A., 1991, AJ 102, 1715
Buta R., Crocker D.A., 1993, AJ 105, 1344
Buta R., Purcell G.B., Crocker D.A., 1995, AJ 110, 1588
Byrd G., Rautiainen P., Salo H., Buta R., Crocker D.A., 1994, AJ 108, 476
Combes F., Elmegreen B.G., 1993, A&A 271, 161
Combes F., Gerin M., 1985, A&A 150, 327
Combes F., Sanders R.H., 1981, A&A 96, 164
Debattista V.P., Sellwood J.A., 1997, preprint
van Driel W., Buta R., 1991, A&A 245, 7
Duval M. F., Athanassoula E., 1983, A&A 121, 297
Elmegreen B.G., 1996, In: Buta R., Crocker D.A., Elmegreen B.G. (eds.) Barred Galaxies. IAU Colloquium 157, ASP, San Francisco, p. 197
Elmegreen B.G., Elmegreen D.M., 1985, ApJ 288, 438
Elmegreen B.G., Elmegreen D.M., 1989, ApJ 342, 677
Elmegreen B.G., Elmegreen D.M., Montenegro L., 1992a, ApJS 79, 37
Elmegreen D.M., Elmegreen B.G., 1995, ApJ 445, 591
Elmegreen D.M., Elmegreen B.G., Combes F., Bellin A.D., 1992b, A&A 257, 17
Friedli D., Benz W., 1993, A&A 268, 65
Friedli D., Benz W., 1995, A&A 301, 649
Friedli D., Martinet L., 1993, A&A 277, 27
Friedli D., Wozniak H., Rieke M., Martinet L., Bratschi P., 1996, A&AS 118, 461
Hunter J.H., Ball R., Huntley J.M., England M.N., Gottesman S.T., 1988, ApJ 324, 721
Lin C.C., Lowe S.A., 1990, Annals N.Y. Acad. Sciences 596, 80
Lindblad P.A.B., Kristen H., 1996, A&A 313, 733
Lindblad P.A.B., Lindblad P.O., Athanassoula E., 1996, A&A 313, 65
Little B., Carlberg R.G., 1991, MNRAS 250, 161
Maciejewski W., Sparke L.S., 1997, ApJ 484, L117
Martin P., 1995, AJ 109, 2428
Masset F., Tagger M., 1997, A&A 322, 442
Moore E.M., Gottesman S.T., 1995, ApJ 447, 159
Noguchi M., 1987, MNRAS 228, 635
Noguchi M., 1996, ApJ 469, 605
Norman C.A., Sellwood J.A., Hasan H., 1996, ApJ 462, 114
Ostriker J.P., Peebles P.J.E., 1973, ApJ 186, 467
Patsis P.A., Athanassoula E., Quillen A.C., 1997, ApJ 483, 731
Raha N., Sellwood J.A., James R.A., Kahn F.D. 1991, Nat 352, 411
Salo H., 1991, A&A 243, 118
Salo H., Laurikainen E., 1993, ApJ 410, 586
Salo H., Rautiainen P., Buta R., et al., 1999, AJ 117, 792
Sanders R.H., Huntley J.M., 1976, ApJ 209, 53
Schwarz M.P., 1981, ApJ 247, 77
Sellwood J.A., 1981, A&A 99, 362
Sellwood J.A., 1985, MNRAS 217, 127
Sellwood J.A., 1987, ARA&A 25, 151
Sellwood J.A., 1993, PASP 105, 648
Sellwood J.A., Athanassoula E., 1986, MNRAS 221, 195
Sellwood J.A., Sparke L.S., 1988, MNRAS 231, 25p
Sellwood J.A., Wilkinson A., 1993, Reports on Progress in Physics 56, 173
Sygnet J.F., Tagger M., Athanassoula E., Pellat F., 1988, MNRAS 232, 733
Tagger M., Sygnet J.F., Athanassoula E., Pellat R., 1987, ApJ 318, L43
Toomre A., Toomre J., 1972, ApJ 178, 623
White R.L., 1988, ApJ 330, 26
Wozniak H., Friedli D., Martinet L., Martin P., Bratschi P., 1995, A&AS 111, 115